ACS OMEGA

http://pubs.acs.org/journal/acsodf

Article

Experimental Kinetic Evaluation of Carbon Dioxide Hydrate-Based Concentration for Grape, Pineapple, and Bitter Melon Juices

Nkululeko Nkosi, Diakanua Nkazi, and Kaniki Tumba*

Cite This: *ACS Omega* 2022, 7, 44591−44602

Read Online

ACCESS | Metrics & More | Article Recommendations | Supporting Information

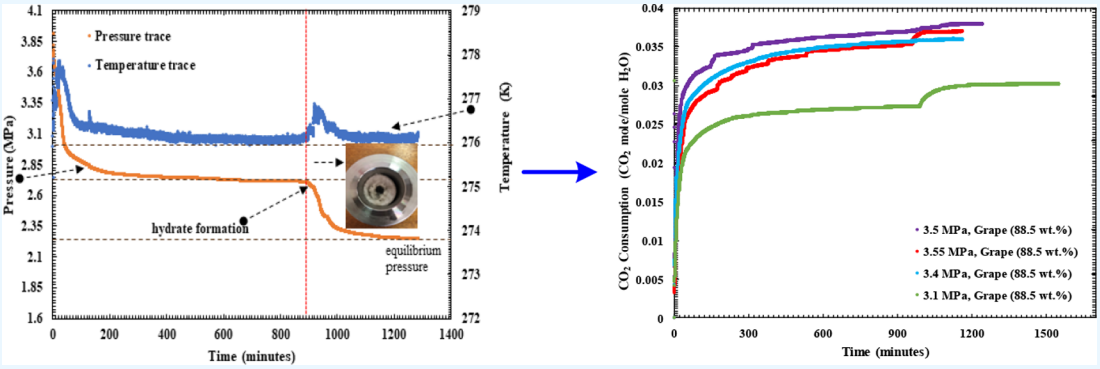

ABSTRACT: Hydrate-based technology has emerged as a promising approach to address the industry's energy demands and product quality challenges in the food industry. Despite reported successes in the literature where higher dehydration ratios were achieved, technological problems like slow formation rates and poor process scale-up economics need to be addressed. Moreover, with little hydrate formation data available, the major focus is on the technology's ability to remove water content, but studies on the kinetics of hydrate formation are scarce. In the present work, the effects of varying grape/pineapple/bitter melon juice water cuts (88.5 to 97.4 ± 2.53 wt %) on the formation kinetics of carbon dioxide (CO_2) hydrates were investigated. Such information can provide insight into the possibile commercialization of the hydrate-based technology. The reported experimental data were determined using the isochoric pressure-search method in a high-pressure reactor at a target initial temperature from 274.15 to 276.15 K and varying initial pressures. Kinetic parameters were calculated using the relative kinetic models proposed in the literature. Lower relative values of investigated kinetic parameters and longer induction times were obtained at lower juice water cuts and lower degrees of subcooling. Despite observed inhibition effects, the study provides useful experimental and modeled kinetic data for filling the knowledge gap in understanding the controlling mechanism of CO_2 hydrate formation. Therefore, it is believed that the reported findings may highlight some important practical aspects related to CO_2 hydrate technology as an alternative juice concentration process.

1. INTRODUCTION

Sustainable and smart nation development requires energy as a critical resource. In the next 20 years, the global energy demand is projected to increase by about 27%, and more fossil fuel resources will be needed for energy supply.[1,2] Meanwhile, the most significant challenge for industries is currently the decline in available fossil fuel reserves. Moreover, as the global energy demand is expected to increase, the impact of greenhouse gases will also increase. Therefore, the greenhouse effect, diminishing fossil fuels, and increased energy demands are pervasive global challenges due to the growing global population. This has increased the demand for agricultural commodities and industrial products. The aforementioned global challenges are becoming more severe and have drawn more attention in different sectors in the past decades.[3−5]

While the depletion of fossil fuel reserves is observed, carbon dioxide emitted by burning fossil fuels for energy purposes is the most prevalent contributor to the greenhouse effect. Even with cost-competitive renewable energy sources, fossil fuels will continue to supplement the energy supply. Furthermore, rapidly developing countries do not appear to be particularly interested in reducing their use of relatively cheap coal reserves. Based on projections, fossil fuels will likely dominate energy mix worldwide for a long time, and renewable energy sources will have difficulties to fully gain a substantial share of the global market.[6,7] Even in the context of the coronavirus

Received: March 31, 2022
Accepted: June 6, 2022
Published: November 30, 2022

https://doi.org/10.1021/acsomega.2c01983
ACS Omega 2022, 7, 44591−44602

Table 1. CAS Registry Number and Purity of the Chemicals

component	CAS reg. no.	supplier	mass fraction	conductivity[b]/μS cm^{-1} this work	conductivity[b]/μS cm^{-1} literature[32]	measurement method
water	7732-18-5	authors' laboratory		0.055	0.055	conductivitymeter
carbon dioxide	124-38-9	Afrox, South Africa	>0.999[a]			none

[a]Purity provided by Afrox. [b]At 298.15 K.

disease (COVID-19) pandemic having caused a shock to the overall energy demand driven by a decline in commercial and industrial activities, carbon emissions kept on increasing.[2,8] In addition, due to the global economy shutdown, this COVID-19 outbreak has significantly increased the unemployment rate to 34.9% in South Africa, leading to energy poverty.[9−11] Therefore, for these reasons, researchers seek alternative methods to reduce carbon emissions while protecting consumers' basic energy needs. Addressing both energy inefficiency and CO_2 emissions represents an integrated approach in developping state-of-the-art innovative technologies.[1,12,21−30,13−20] As for the fruit processing industry, carbon dioxide hydrate-based juice concentration has become increasingly popular as a novel approach for carbon dioxide reuse (i.e., reduction of CO_2 emissions) and energy savings.

Nowadays, the food industry utilizes freeze concentration as an alternative to evaporation to remove water from heat-sensitive solutions and preserve bioactive contents. Concentration via hydrate formation is similar to freeze concentration such that the ice formation step is replaced with gas hydrate crystal formation in the former technology. The principle behind both processes is that the components of juice, except water, are not involved in the crystal structure of either ice or gas hydrates. The freeze concentration process is very energy-intensive in the food industry as it relies on temperatures below the water freezing point. However, energy requirements in gas hydrate-based technology are moderate since gas hydrates can be formed above the water freezing point. Therefore, to conserve energy without destroying bioactive components in liquid foods such as juices[21,22,34,23−26,28,31−33] and coffee,[29,35,36] it is feasible to incorporate high concentrations of CO_2 into liquid foods and effect water removal through a hydrate-based technology. Hence, CO_2 hydrate-based technology in the food industry has emerged as a green solution to guarantee stable and sustainable renewable energy utilization.

Although the hydrate-based concentration technology offers energy conservation and preservation benefits in the fruit juice concentration industry, its commercialization associated with industrial-scale production is not yet effective. This does not come as a surprise when it appears that thermodynamic and kinetic data relevant to hydrate-forming systems in the presence of fruit juices are scarce. Such data are instrumental in designing and optimizing industrial processes. The present experimental study was initiated to provide new experimental data from which insight can be gained into the interplay between hydrate formation kinetics and juice water contents. It was reported in previous studies that gas hydrate formation depended on juice composition, the mixing of the phases, and system geometry.[21,25,37] Kinetic studies entail determining key kinetic parameters of hydrate formation, including storage capacity, apparent rate constants, water-to-hydrate conversion, gas consumption, and rates. These kinetic parameters of gas hydrate formation are of interest in fully assessing the proposed concentration process of gas hydrates in vew of its future commercialization. Well-known kinetic models proposed by Englezos et al.[38] were used in this study to determine these kinetic parameters. Based on the crystallization theory,[38] these kinetic models were developed to calculate the difference between the fugacity of the gas species in the hydrate and vapor phases. This is the driving force for gas hydrate formation.

Concretely, experimental kinetic data under hydrate formation conditions have been reported for three different systems containing carbon dioxide, water, and grape/pineapple/bitter melon juices. The effects of grape/pineapple/bitter melon juice water cuts on experimentally obtained induction time and calculated kinetic parameters have been examined at various initial temperatures and pressures.

2. EXPERIMENTAL SECTION

2.1. Materials. Ultrapure Millipore-Q water, fruits, and carbon dioxide (CO_2) were used for the present study. The laboratory-obtained water with an electrical resistivity of 18.2 MΩ cm at 298.15 K was used for this experiment. Table 1 contains additional information about these two chemicals.

Afrox (South Africa) provided CO_2 gas with a minimum mass fraction of 99.99%, and raw fruits (grape, pineapple, and bitter melon) were purchased from Food lovers supermarket in KwaZulu-Natal (South Africa, Durban). Fresh juice was extracted from these fruits by carefully crushing them; the characteristics of their compositions are given in Table 2, which will be discussed further in the Results and Discussion section.

Table 2. Composition of Investigated Bitter Melon, Grape, and Pineapple Juice[c]

proximate	quantity (mean ± SD, mg/100 g)	
water content[a]	96.5 ± 2.53[d]	97.4 ± 2.53[d]
	88.5 ± 2.53[e]	91.4 ± 2.53[e]
	91.1 ± 2.53[f]	93.3 ± 2.53[f]
total solids[a]	3.5 ± 0.02[d]	2.6 ± 0.02[d]
	11.5 ± 0.02[e]	8.6 ± 0.02[e]
	8.9 ± 0.02[f]	6.7 ± 0.02[f]
total ash[a]	0.386 ± 0.043[d]	0.307 ± 0.043[d]
	0.263 ± 0.043[e]	0.217 ± 0.043[e]
	0.216 ± 0.043[f]	0.168 ± 0.043[f]
lipids	2.3 ± 0.01[d]	1.83 ± 0.67[d]
	5.93 ± 0.67[e]	4.78 ± 0.67[e]
	7.81 ± 0.01[f]	5.85 ± 0.67[f]
pH[b]	4.31 ± 0.01[d]	4.42 ± 0.01[d]
	3.92 ± 0.01[e]	4.42 ± 0.01[e]
	3.72 ± 0.01[f]	4.12 ± 0.01[f]
ascorbic acid (vitamin C)	68.58 ± 3.16[d]	53.81 ± 3.16[d]
	18.55 ± 0.92[e]	13.45 ± 3.16[e]
	15.4 ± 0.87[f]	11.95 ± 3.16[f]

[a]Expressed as (wt %). [b]Expressed as the pH scale. [c]AOAC International.[39] [d]Bitter melon juice. [e]Grape juice. [f]Pineapple juice.

https://doi.org/10.1021/acsomega.2c01983
ACS Omega 2022, 7, 44591−44602

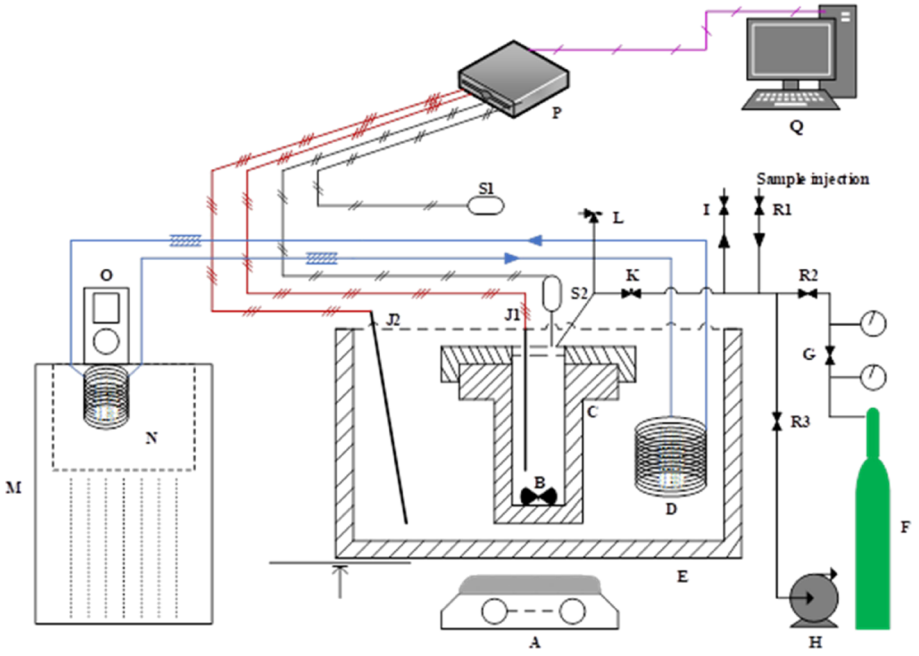

Figure 1. Schematic diagram for the high-pressure equilibrium apparatus. A, magnetic stirrer; B, neodymium magnet stir bar; C, high-pressure equilibrium cell; D, cooling coil; E, thermos-statted bath; F, gas cylinder; G, pressure regulator; H, vacuum pump; I, vent valve; J (1 or 2), temperature probe (Pt-100); K, needle valve for loading; L, relief valve; M, LTC4 unit; N (LTC4 unit), built-in circulating bath; O, circulating thermostat; P, data acquisition system; Q, computer; R (1,2 or 3), shut-off valve; S (1 or 2), pressure transducer.

The preparation of juice solutions with an uncertainty level of ±0.5 mL gravimetrically was conducted using an accurate analytical balance, model AS220/C/2 (provided by RADWAG, Poland) having an uncertainty of ±0.0001 g in mass.

2.2. Apparatus. In this study, a high-pressure equilibrium cell was used. A 100 mL stainless-steel container made from stainless steel (SS 316L) was supplied by Büchi, Switzerland. A nickel−chromium−iron−molybdenum alloy is hydrophobically coated on the inside of the cell, making it capable of withstanding temperatures and pressures up to 473.15 K and 10 MPa, respectively. The liquid bath and system temperatures were measured with a four-wire Pt-100 thermocouple (supplied by Grant Instruments, United Kingdom), with an error of ±0.3 K. An inside pressure of the high-pressure equilibrium cell was measured with a pressure transducer (supplied by ESI Technology of the United Kingdom), with an uncertainty of 0.25% of full scale. A magnetic stirrer bar was used with a capacity of 1000 RPM to stabilize the thermodynamic equilibrium quickly and ensure thorough mixing of contents. A temperature-control unit, designated LTC4 (supplied by Grant Instruments, United Kingdom), was composed of a TX150 Optima circulation bath and an R4 storage tank and refrigeration unit. A liquid bath and system temperature were set and controlled with this device. An aqueous solution of glycerol water served as the cooling solution. The cell is vacuumed to remove any trapped air (supplied by Gardner Denver, United States). In SquirrelView software, pressure and temperature data at particular intervals were monitored using the apparatus connected to a Grant Instruments Data Acquisition Unit (SQ2020-1F8). Figure 1 shows a schematic diagram of the experimental setup utilized in this study.

3. EXPERIMENTAL METHODS

3.1. Kinetics of Hydrate Formation Measurements. In this study, for this thermodynamic measurement, the same experimental method and experimental procedure used in the literature as described by Sloan and Koh,[40] Tumba et al.,[41] and Fakir et al.[42] for hydrate measurements were used. However, the primary purpose for these measurements was to estimate the effect of each parameter used (i.e., initial temperature and pressure as well as fruit juice concentration) and identify the hydrate formation and growth rate, storage capacity, mole consumption, apparent rate constant, and water-to-hydrate conversion during the hydrate formation.

In these measurements, the system for each run was washed vigorously to eliminate any remaining fruit juice sample from previous kinetic measurements, and a fresh fruit juice sample at selected concentration was used. The equilibrium cell was cleaned with soapy liquid and repeatedly rinsed with ultrapure Millipore water. Then, the system was soaked with methanol or ethanol for 30 min. After this, the cell was rinsed with acetone to ensure that it was dry before each experimental run. After cleaning, the equilibrium cell cover plate was tightened to ensure proper seal before being pressurized and was connected to the monitoring system. Then, a vacuum pump was used to evacuate the cell for approximately 30 min to a pressure of 0.00025 MPa. After this, the appropriate quantity (40 mL with an uncertainty level of ±0.5 mL) of the fruit juice sample freshly prepared was injected into the equilibrium cell. Again, the equilibrium cell was evacuated to eliminate any presence of air for 5 min. Afterward, the equilibrium cell was submerged into the temperature-controlled liquid bath set for the desired initial temperature to cool the equilibrium cell for at least 45 to 90 min depending on the liquid sample to ensure that the equilibrium temperature was achieved.

When the system temperature stabilizes, the equilibrium cell was purged by slowly pressurizing with CO_2 to 0.5 MPa. Then,

https://doi.org/10.1021/acsomega.2c01983
ACS Omega 2022, 7, 44591−44602

the cell was vented completely. This cycle was repeated at least three times to prevent residual air contamination. The cell was then pressurized slowly with CO_2 to a desired initial pressure within the hydrate stability zone. During CO_2 injection, the dissolution of warm CO_2 in water causes a slight increase in the system temperature. After pressurizing the cell, the pressure-regulating valve was closed, and the magnetic stirrer was switched on and set at a speed of 500 rpm to agitate the phase inside the equilibrium cell. Then, the system temperature decreases steadily to the set temperature. The system temperature and pressure were monitored and recorded by a data acquisition connected to a computer installed with the SquirrelView software for display until an equilibrium condition was reached. Since heat energy is released (exothermic process) during hydrate formation, the nucleation point was detected by a spiked system temperature (in both the interphase and the liquid), depicted in Figure 2. Then, as

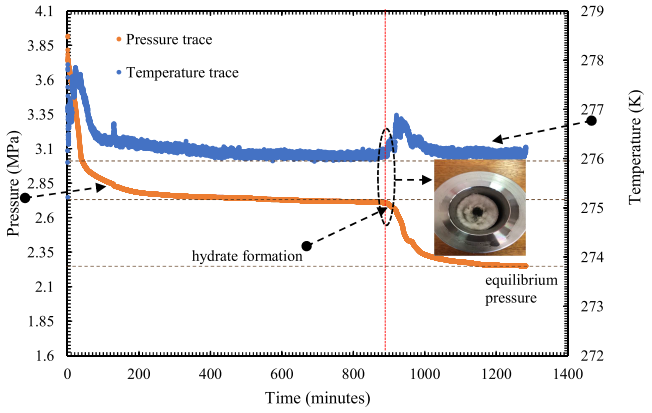

Figure 2. Pressure and temperature traces during the hydrate nucleation and growth at a constant temperature and initial pressure of 276.15 and 3.9 MPa in grape juice having 50.0 vol % of Millipore water added. As can be seen in photograph (i), the hydrate formed by the experiment.

the hydrate was formed, CO_2 was encapsulated (hydrate growth) inside the crystals, causing the cell pressure to drop sharply. The system was left until a stable temperature and pressure were observed after the hydrate growth.

In order to shut the system down after the pressure stabilizes, the data acquisition was stopped, and the stirrer, the temperature controller, and the bath were turned off. Next, the cell was disconnected from the data acquisition system, removed from the liquid bath, and placed in a fume hood. The gas accumulated inside the cell was slowly released through the vent, and the contents were discarded. Finally, the cell was cleaned as described above. All measurements were repeated twice to ensure that the reported results were reproducible and accurate, and the uncertainty of the induction time reported is ±1 min.

4. THEORY

4.1. Kinetic Models. In this study, kinetic parameters were empirically determined, including the rate of hydrate formation, storage capacity, apparent rate constant, water-to-hydrate conversion, and gas consumption. The kinetic models developed by Englezos et al.[38] were used and are well described in Sloan and Koh's literature.[40] For the formation of CO_2 gas hydrates in juice systems investigated, the following equation describes the physical reaction between water and CO_2 gas:

$$CO_2 + nH_2O \rightarrow CO_2 \cdot nH_2O \tag{1}$$

where n denotes the hydration number calculated by utilizing the following equation for structure I.[40]

$$n = \frac{46}{6\theta_L + 2\theta_S} \tag{2}$$

where θ_L and θ_S denote the fractional occupancy and indicators of L and S, which represent large and small cavities, respectively. In this study, the model parameters for the Langmuir constants for CO_2 gas were determined using the Parrish and Prausnitz[43] equation, as shown below:

$$C_{ij} = \frac{A_{ij}}{T}\exp\left(\frac{B_{ij}}{T}\right) \tag{3}$$

where A_{ij} and B_{ij} are adjustable adsorption parameters found for different hydrate formers in the open literature.[43] According to Chen and Guo,[44] the following equation is used to calculate the fugacity of gas species in the vapor phase:

$$f_g = f^o(1-\theta)^{\alpha'} \tag{4}$$

$$\alpha' = \frac{\lambda_1}{\lambda_2} \tag{5}$$

where f denotes species' fugacity in equilibrium with the vapor phase, while subscript "o" represents its fugacity in equilibrium with the unfilled initial hydrate phase. According to this equation, the symbols "λ_1" and "λ_2" denote the number of related cavities per water molecule and the number of gas hydrate formers per water molecule, respectively. These assumptions, α' in eq 5, lead to 1/3 and 2 for structures I and II, respectively.[44] Using eq 6, one can calculate the fugacity of a gas molecule in equilibrium with a basic unfilled hydrate:

$$f^o = f^o(T) f^o(P) f^o(a_w) \tag{6}$$

where

$$f^o(T) = A\exp\left(\frac{B}{T-C}\right) \tag{7}$$

$$f^o(P) = A\exp\left(\frac{\beta' P}{T}\right) \tag{8}$$

$$\beta' = \frac{\Delta V}{\lambda_2 R} \tag{9}$$

$$f^o(a_w) = 1 \tag{10}$$

T and P in the above equations are in K and Pa, respectively. In eq 7, the A, B, and C parameters represent the Antoine constants for the hydrate former.[44] For structure I, the β' parameter is equal to 0.4242×10^{-5} (K/Pa), and for structure II, it is equal to 1.100224×10^{-5} (K/Pa).[44] According to Langmuir's adsorption theory, the θ parameter can be calculated as follows:

$$\theta_i = \frac{Cf_g}{1 + Cf_g} \tag{11}$$

https://doi.org/10.1021/acsomega.2c01983
ACS Omega 2022, 7, 44591−44602

Table 3. Experimental Kinetic Results of Hydrate Formation in the Presence of Bitter Melon Juice[a]

WC[b]/(wt %)	T_{exp}[c]/(K)	ΔT_{exp}[d]/(K)	P_{exp}[e]/(MPa)	IT[f]/(min)	SC[g]/(v/v)	FMGC[h] mmole	FWHC[i]/(%)	K_{app}[j] × 10^9	HFR[k] × 10^3
96.5	274	4.09	2.9432	783.58	128.95	0.023	27.60	18.5	4.12
		4.65	3.2371	292.08	145.57	0.027	32.40	20.5	11.5
		4.83	3.3293	97.75	162.85	0.029	34.80	21.1	13.3
	275	3.45	3.1131	892.92	109.61	0.023	27.39	17.6	7.70
		4.15	3.5063	301.33	127.29	0.027	31.81	20.0	12.6
		5.05	4.0739	115.08	133.59	0.028	33.38	23.4	22.2
	276	2.75	3.2826	890.25	86.91	0.018	21.72	17.2	3.18
		3.15	3.4736	556.92	113.19	0.024	28.28	18.3	9.71
		3.65	3.7934	183.01	121.82	0.025	30.46	20.0	11.3
97.4	274	5.15	3.0533	83.92	135.35	0.028	50.4	18.8	12.6
		6.05	3.4888	46.25	83.43	0.038	68.4	21.7	18.9
		6.45	3.7120	4.58	101.36	0.041	73.76	23.1	26.4
	275	3.75	2.8968	115.42	105.54	0.022	39.56	17.4	8.16
		4.91	3.3897	71.08	158.22	0.033	59.31	20.5	16.9
		5.75	3.9080	12.08	197.94	0.008	14.22	23.9	22.6
	276	2.75	2.8916	1167.67	93.52	0.018	27.28	14.1	5.04
		3.34	3.1375	443.25	109.28	0.023	40.96	15.4	7.41
		4.25	3.5720	184.17	158.47	0.033	59.4	17.7	13.4
100	275[l]	3.42	3.0000	1.10	174.25	0.166	27.02	258.8	102
	276[m]	2.65	3.0600		49.90	0.042	26.90	3.57	11.0

[a]Standard uncertainty: $u(T)$ = 0.08 K, $u(P)$ = 0.0234 MPa. [b]Water content. [c]Initial temperature. [d]Degree of subcooling. [e]Initial pressure. [f]Induction time. [g]Storage capacity. [h]Final moles of gas consumed per moles of water. [i]Final water-to-hydrate conversion (mole%). [j]Apparent rate constant. [k]Hydrate formation rate. [l]Mohammadi et al.[46] [m]Abedi-Farizhendi et al.[29]

where C_i indicates the Langmuir constant previously determined (eq 3) and f_g is the fugacity of gas in the vapor phase. In order to calculate the amount of gas consumed through clathrate hydrate formation, the real gas law is used as follows:[42,45]

$$\Delta n_g = \frac{P_0 V_0}{Z_0 R T_0} - \frac{P_t V_t}{Z_t R T_t} \tag{12}$$

where P, T, and V signify the pressure, temperature, and volume of gas inside the high-pressure equilibrium cell. For each time value of 0 and t, the subscripts indicate the equilibrium conditions at that time. In eq 4, SRK EoS is used to estimate the compressibility factor, Z, of the guest's molecule.[45] Based on the following equation,[46] the gas volume inside the cell, V_t, at time t can be estimated:

$$V_t = V_{cell} - V_{S_o} + V_{RW_t} - V_{H_t} \tag{13}$$

where V_{cell} represents the cell's total volume, which is 100 cm^3, and V_{So} represents the volume of the aqueous solution, which is 40 cm^3. Then, the volume of solution or water reacted, V_{RWt}, at a time t is estimated using the following equation:[46]

$$V_{RW_t} = n \times \Delta n_g \times v_w^L \tag{14}$$

where v_w^L represents the molar volume of water in the cell, which can be calculated by the following expression:[38,46]

$$v_w^L = 18.015 \times 1 - 1.0001 \times 10^{-2} + 1.33391 \times 10^{-4} \times (1.8(T - 273.15) + 32) + 5.50654 \times (1.8(T - 273.15) + 32)^2 \times 10^{-3} \tag{15}$$

where T and v_w^L are in K and m^3/mol, respectively. The molar volume, V_{Ht}, of the hydrate at time t, is calculated as follows:[46]

$$V_{H_t} = n \times \Delta n_g \times v_w^{MT} \tag{16}$$

where T is in K, P is in MPa, and v_w^{MT} is the volume of the empty hydrate lattice. According to Klauda and Sandler[47] and Dharmawardhana et al.,[48] the following equations can be used to calculate molar volume (v_w^{MT}) in structure I's empty hydrate lattice phase:

$$v_w^{MT} = (17.13 + 2.249 \times 10^{-5} T + 2.013 \times 10^{-6} T^2) \times \left(\frac{10^{-30} N_A}{46}\right) - 8.006 \times 10^{-9} P + 5.448 \times 10^{-12} P \tag{17}$$

where N_A is Avogadro's number and v_w^{MT}, T, and P are in m^3/mol, K, and MPa, respectively. Water-to-hydrate conversion (known as a mole of water per moles of feed solution) is calculated as follows:

$$\text{water-to-hydrate conversion} = \frac{n \times \Delta n_g}{n_{w_o}} \tag{18}$$

The storage capacity of gas hydrates is defined as the volume of gas they can store under standard pressures and temperatures. The equation (eq 19) for calculating the storage capacity of hydrate formers during hydrate formations[46] is used as follows:

$$SC = \frac{V_{STP}}{V_H} = \frac{\Delta n_g R T_{STP}/P_{STP}}{V_H} \tag{19}$$

where subscript STP stands for the standard conditions, and V_H is the molar volume of hydrate formation, which is calculated using eq 16. As a result of the formation of gas hydrates, the following equation is used to estimate the rate of gas consumption:[38,46,49]

$$r(t) = \frac{n_{g,i-1} - n_{g,i+1}}{(t_{i-1} - t_{i+1}) n_{w_o}} = k_{app}(f^g - f^g_{equilib.})_{t_i} \tag{20}$$

https://doi.org/10.1021/acsomega.2c01983
ACS Omega 2022, 7, 44591−44602

Table 4. Experimental Kinetic Results of Hydrate Formation in the Presence of Grape Juice[a]

WC[b]/(wt %)	T_{exp}[c]/(K)	ΔT_{exp}[d]/(K)	P_{exp}[e]/(MPa)	IT[f]/(min)	SC[g]/(v/v)	FMGC[h]	FWHC[i]	K_{app}[j] × 10^9	HFR[k] × 10^3
88.5	274	5.15	3.3338	458.05	143.30	32.27	0.029	16.3	25.1
		5.85	3.6529	90.17	157.10	38.20	0.032	18.5	28.4
		5.85	3.6680	47.92	158.39	39.10	0.033	18.6	29.1
	275	3.25	2.9690	1269.92	105.51	26.36	0.022	12.6	16.3
		4.55	3.5651	507.42	133.26	32.01	0.028	16.3	25.7
		4.75	3.6282	287.92	140.21	33.32	0.029	16.7	27.1
		5.25	3.8767	122.33	144.70	35.73	0.030	18.2	28.1
		5.35	3.9391	53.08	155.08	39.01	0.031	18.7	29.4
	276	2.65	3.1126	1820.33	98.50	24.61	0.021	12.2	14.2
		3.65	3.5736	1193.1	110.91	27.72	0.023	14.8	19.4
		4.25	3.9184	882.75	151.63	37.89	0.032	16.8	25.2
91.4	274	2.75	2.1382	23.75					
		4.75	2.8866	16.08					
		6.75	3.8245	11.17					
		6.75	3.8342	6.67					
		7.15	4.1001	2.92					
	275	4.17	3.0795	990.25	126.77	47.52	0.026	14.7	20.3
		4.95	3.4774	308.67	141.95	64.80	0.036	17.4	29.3
		5.05	3.5146	191.08	152.18	66.60	0.037	17.7	31.4
		5.15	3.5451	146.75	157.48	68.40	0.038	17.9	32.7
	276	3.15	3.0321	425.86	113.84	42.67	0.024	13.0	16.7
		3.87	3.4129	342.92	140.91	52.82	0.029	15.4	22.2
		4.15	3.4983	298.33	160.28	60.08	0.033	15.9	24.2
		4.54	3.7202	71.5	174.51	65.41	0.036	17.3	26.7
100	275[l]	3.42	3.0000	1.10	174.25	0.166	27.02	258.8	102
	276[m]	2.65	3.0600		49.90	0.042	26.90	3.57	11.0

[a]Standard uncertainty: $u(T)$ = 0.08 K, $u(P)$ = 0.0234 MPa. [b]Water content. [c]Initial temperature. [d]Degree of subcooling. [e]Initial pressure. [f]Induction time. [g]Storage capacity. [h]Final moles of gas consumed per moles of water. [i]Final water-to-hydrate conversion (mole%). [j]Apparent rate constant. [k]Hydrate formation rate. [l]Mohammadi et al.[46] [m]Abedi-Farizhendi et al.[29]

Table 5. Experimental Kinetic Results of Hydrate Formation in the Presence of Pineapple Juice[a]

WC[b]/(wt %)	T_{exp}[c]/(K)	ΔT_{exp}[d]/(K)	P_{exp}[e]/(MPa)	IT[f]/(min)	SC[g]/(v/v)	FMGC[h]	FWHC[i]	K_{app}[j] × 10^9	HFR[k] × 10^3
91.1	274	6.25	3.1963	137.08	132.97	0.033	33.23	17.5	11.7
		7.35	3.7980	52.83	165.49	0.041	41.35	21.1	12.8
		7.55	3.9086	4.00	173.46	0.043	43.34	21.7	18.4
	275	6.05	3.5764	405.15	136.84	0.034	34.20	17.8	14.3
		6.45	3.8021	139.67	145.82	0.036	36.44	19.0	16.8
		6.95	4.1672	20.08	166.90	0.042	41.71	20.9	20.7
	276	4.75	3.4405	581.67	120.72	0.030	30.16	15.4	7.66
		5.25	3.6976	193.83	131.86	0.033	32.95	16.7	19.1
		5.85	4.1011	34.33	151.30	0.039	38.92	18.6	21.1
93.3	274	5.55	3.1663	129.08	175.00	0.035	62.84	14.8	12.5
		6.35	3.5995	97.58	184.55	0.041	73.23	17.0	23.1
		6.45	3.7277	28.67	193.73	0.043	76.87	17.6	25.3
	275	4.05	2.9725	470.57	154.34	0.032	57.85	15.2	9.21
		4.95	3.4297	396.92	172.05	0.036	64.49	17.7	1.6
		5.45	3.6157	129.17	183.41	0.038	68.75	18.7	20.8
	276	3.35	3.1082	643.92	123.93	0.028	46.45	14.5	6.5
		4.75	3.7869	330.42	135.45	0.027	50.75	18.0	18.9
		4.85	3.8697	242.50	136.35	0.025	51.11	18.3	21.7
100	275[l]	3.42	3.0000	1.10	174.25	0.166	27.02	258.8	102
	276[m]	2.65	3.0600		49.90	0.042	26.90	35.7	11.0

[a]Standard uncertainty: $u(T)$ = 0.08 K, $u(P)$ = 0.0234 MPa. [b]Water content. [c]Initial temperature. [d]Degree of subcooling. [e]Initial pressure. [f]Induction time. [g]Storage capacity [h]Final moles of gas consumed per moles of water. [i]Final water-to-hydrate conversion (mole%). [j]Apparent rate constant . [k]Hydrate formation rate. [l]Mohammadi et al.[46] [m]Abedi-Farizhendi et al.[29]

In eq 20, n_{i-1} and n_{i+1} represent the number of gas molecules in the vapor phase at a time equal to t_{i-1} and t_{i+1}, respectively, where n_{w0} is the initial number of water molecules in the liquid phase, which is estimated using the initial volume of water (40 cm^3 in this study). According to this study, k_{app} (the apparent rate constant of reaction during hydrate formation) is another parameter described. This parameter is estimated using the equation below.[46]

https://doi.org/10.1021/acsomega.2c01983
ACS Omega 2022, 7, 44591−44602

$$k_{app} = \frac{r(t)}{(f^{g} - f^{g}_{equilib.})_{t_i}} \quad (21)$$

5. RESULTS AND DISCUSSION

5.1. Experimental Results and Analysis on the Kinetics of Hydrate Formation. *5.1.1. Time of Carbon Dioxide Hydrate Formation (Induction Time).* A total of 60 hydrate formation experiments were carried out at initial pressures ranging from 2.1382 to 4.8731 MPa and constant temperatures from 274.15 to 276.15 K in three juice-containing systems (system 1: CO_2 + grape juice; system 2: CO_2 + pineapple juice; system 3: CO_2 + bitter melon juice), with pure and dilute fruit juice concentration. All measurements were repeated twice to ensure that the reported results were reproducible and accurate. The uncertainty of the reported induction time is ±1 min. The experimental results are provided in Tables 345. It should be noted that hydrate formation times were calculated by averaging two measurements under identical conditions. It was observed that the required hydrate nucleation time depended on temperature and pressure. Laboratory hydrate dissociation data measurements revealed that hydrate formation was a time-consuming phenomenon, an indication of its energy-intensive nature. Therefore, in the context of techno-economic analysis, hydrate formation time can be regarded as the main factor ensuring the financial viability of the proposed technology. Thus, this factor is so crucial that excluding it may lead to inaccurate models for the design and optimization of hydrate-based fruit concentration processes. It is vital in understanding the kinetics and mechanisms to form gas hydrates for newly investigated systems.

In this study, the hydrate formation time varied from seconds to days due to the complex nature of the hydrate formation process.[40,50] This induction time is determined between gas injection and the occurrence of the nucleate incipient.[40] This occurs due to a dramatic drop and abrupt increase of the system pressure and temperature. This quick temperature increase is due to the heat released when the supersaturated metastable state is suddenly broken. Tables 3−5 report the average induction time values with other pertinent data for newly investigated systems obtained from experimental kinetics of hydrate formation measurements carried out at constant initial temperatures of 274.15 to 276.15 K and different initial pressures ranging from 2.80 to 4.10 MPa.

As reported in Tables 3−5, it can be seen that the incipient hydrate time relied on numerous factors, including initial pressure and temperature, subcooling temperature, juice residuals, water cuts, and system geometry. Therefore, results obtained in this study for investigated systems did not accurately match. This signified that replication of results obtained from one system is not possible. All investigated systems seem to provide better stability gain at higher pressures and temperatures. The assessment of these factors on induction time is discussed later in this paper.

5.1.2. Effect of Initial Pressure and Temperature on Induction Time. Initial conditions (pressure and temperature) were selected in the hydrate stability zone to ensure the clathrate hydrate formation. Before the initial hydrate formation, the hydrate pressures' signal shifts (up to ±0.05 MPa) were observed. Induction times varied significantly with experimental conditions. As observed in Tables 3−5, induction times for the new systems investigated in this study are shorter at high initial pressures. This is understandable as high initial pressures correspond to high degrees of subcooling.

During the dissolution stage between gas injection and the occurrence of nucleation, the pressure was observed to drop, indicating that a large amount of CO_2 was dissolved in the juice system. This was followed by a sudden pressure drop and a sharp temperature increase, indicating the onset of CO_2 hydrate nucleation. It was also observed that clathrate hydrate nucleated immediately once the agitation was initiated at higher degrees of subcooling. This is due to the fact that the liquid phase was quickly converted to the bulk hydrate. The hydrate formation rate increased as the initial pressure was increased. This indicates that at higher initial pressures, the mass transfer resistance in the liquid phase is lower due to an increased driving force for the hydrate formation reaction, resulting in rapid hydrate formation.

When the equilibrium pressure is attained, a condition such that the hydrate is no longer formed, the pressure drop observed in Tables 3−5 may be related to hydrate formation. As it can be seen, increasing the initial pressure and the degree of subcooling as driving forces of the hydrate formation has decreased the pressure drop. This observed behavior may be attributed to the high solubility of CO_2 at a high pressure, which compels the liquid phase to accommodate a limited number of additional CO_2 molecules prior to conversion into hydrates. However, an opposite trend was observed when the system temperature was decreased, leading to a decrease in CO_2 solubility in water and an increased pressure drop. Grape juice exhibited the highest hydrate formation rate, in which more gas in the same period is consumed than pineapple and bitter melon juices.

On the other hand, an increase in the system temperature, which amounts to a decrease in subcooling, results in a further reduction of the induction times. This indicates that it is difficult for the carbon dioxide hydrate to be formed at higher temperatures; the higher the induction time, the slower the hydrate formation rate. However, at lower temperatures, the system reaction time was shortened. This is due to the system's heat transfer resistance, which becomes smaller and enhances the reaction to occur and proceeds rapidly, which conforms to the formation law of hydrates. It appears that favorable conditions for improved kinetics are characterized by low temperatures and high pressures. Under these conditions, energy costs are expected to be exorbitant. Hence, the need to assess the combined effect of these two important factors as a step toward process optimization. This assessment was carried out in the literature by determining the difference between the fugacity (chemical potential) of the guest gas in the hydrate phase and the vapor phase as an alternative driving force.[51] It is discussed later in this paper.

5.1.3. Effect of Water Content on Induction Time. As shown in Tables 3−5, the hydrate formation time was slightly higher for pure juices than that of diluted juices. The high solubility of carbon dioxide reduces the disruption of water−gas interactions due to juice components. In clear terms, due to their very low concentration in water as compared to CO_2, juice components have no significant effect on hydrate formation time. This observed increase in induction time was expected. It is consistent with the reported inhibition mechanism attributed to the perturbation of water—the

https://doi.org/10.1021/acsomega.2c01983
ACS Omega 2022, 7, 44591−44602

increase in inhibition effects of investigated systems on hydrate formation, resulting in a less pressure drop.

Regarding effectiveness as kinetic hydrate inhibitors, grape juice inhibits the hydrate formation less notably than pineapple and bitter melon juice by presenting the shortest induction time for the studied conditions. This tendency is followed by pineapple and bitter melon juice. More hydrates were formed for juice systems with the highest initial quantity of water addition (91.1, 93.3, and 97.4 wt %). Moreover, considerable delays in the induction time values were observed for pure juice samples (88.5, 91.1, and 96.5 wt %). Conversely, a comparison between diluted (91.4, 93.3, and 97.4 wt %) and pure juice samples (88.5, 91.1, and 96.5 wt %) revealed that the induction time values of the 91.4, 93.3, and 97.4 wt % juice samples were faster. This was expected since the inhibiting effects were weakened.

5.2. Impact of Initial Conditions on Kinetic Parameters of Formation for Carbon Dioxide Hydrates. *5.2.1. The Rate of Hydrate Formation and Growth with Different Water Cuts.* In this study, the hydrate formation rate for each investigated system was measured as a kinetic parameter for hydrate formation. The effect of initial pressure conditions at different concentrations of investigated juices on the amount of gas consumed at constant temperatures is listed in Tables 3−5 and plotted in Figures S1−S3 (Supplementary Material), allowing easier visualization.

The hydrate formation rate or growth experiments with or without water addition indicated the impact of inhibiting effects reported in previous sections. The inhibition effects were observed with investigated systems at temperatures 274.15 to 276.15 K and varying system pressure. For all investigated systems at each constant temperature, it was observed that the maximum hydrate formation rate occurred at the beginning of the hydrate formation stage, and then, the rate decreased. This observed behavior may be interpreted by considering two factors. As the gas molecules increase and become clustered inside the hydrate cavities, they cause a significant reduction of CO_2 gas in the vapor phase. Second, as hydrate formation takes place in a closed system, water consumed during this process causes the high-concentration CO_2 gas to diffuse faster from saturated vapor to a hydrate-forming phase, resulting in a significant decrease of pressure. This reduction in pressure increased the rate of hydrate formation.

Figures S1−S3 show that the hydrate formation rate increased with the increasing system pressure. However, a reverse effect on the rate of hydrate formation was observed for the system temperature. This is due to a decreased degree of subcooling of hydrates. Thus, the formation rate decreases accordingly. Moreover, the best results were obtained at a higher degree of subcooling for juice systems with added water compared to pure juice. This observed behavior could be due to an increased surface tension of water caused by increased CO_2 solubility in water. This was observed in all investigated juice systems. Notably, the change in experimental conditions indicated is indistinguishable in all appended figures.

5.2.2. The Amount of Gas Consumption and Rate of Gas Uptake with Different Water Cuts. The gas consumption rate for each investigated system was experimentally determined as a kinetic parameter for hydrate formation. This kinetic parameter was used to study the hydrate growth process using a kinetic model proposed by Englezos et al.[38] The effect of initial pressure conditions at different concentrations of investigated juices on the amount of gas consumed at constant temperatures is shown in Tables 3−5 and plotted in Figures S4−S6 (Supplementary Material), allowing easier visualization.

As it can be seen in these figures, the CO_2 consumption rate increased with the initial pressure at a constant temperature in all three systems. At an increased initial pressure, the metastable state is broken in which CO_2 gas is consumed rapidly, leading to a fast decrease of pressure until an equilibrium state is reached.

Moreover, these tabulated data demonstrated that the enormous gas consumption was obtained at higher subcooling, while the lowest was obtained at lower subcooling. On the other hand, raising the system temperature from 274.15 to 276.15 K, which correlates with a reduction in subcooling, resulted in a slight increase in hydrate nucleation time and the lowest gas consumption rate. This indicates the strong influence of system temperature, suggesting that higher temperatures (e.g., 276.15 K) may not be used without losing efficiency. At this temperature, for practical application, it was observed that the CO_2 gas consumption rates are enhanced when higher pressure values are used. Therefore, due to the high-pressure requirements needed from the compressor, this may represent energy loss for the proposed hydrate-based process for juice concentration. Thermodynamically, this temperature effect may be attributed to the solubility of CO_2 in water, which is an important parameter. It is reported in the literature that the solubility of CO_2 increases with a decrease in system temperature. These results were expected since the set temperature is low, resulting in higher solubility of CO_2 and, theoretically, a higher crystal growth rate.

Conversely, clathrate hydrate was formed very fast under higher initial conditions. As a result, a small amount (approximately equal to zero) of CO_2 gas was consumed during the hydrate formation process. At this moment, when the driving force is null, the system is near equilibrium, no further gas is consumed (constant pressure and temperature), and the clathrate hydrate formation process is considered complete. This observed behavior may be attributed to various aspects, including the driving force and higher vapor−hydrate interface area. The equilibrium pressure is small at a high driving force (i.e., initial pressure or degree of subcooling). At the higher vapor−hydrate interface, most CO_2 is transferred directly into the hydrate phase while minimizing CO_2 gas dissolving in the liquid phase, reducing the gas path to cages.

Experiments revealed that pure juice's presence in all systems presented the lowest CO_2 consumption, while those with added water showed the highest consumption due to the increased amount of free water that makes hydrate cages. For the pure juice system, it was observed that the supersaturation degree was small. As a result, the moles of CO_2 consumed are reduced due to less-encapsulating CO_2 molecules into hydrate cavities. This hypothesis may be related to the relatively high induction time presented by these inhibiting effects in the experiments. In terms of gas consumption rate efficiency for CO_2, this indicates that the CO_2 + bitter melon system could be more appropriate for this proposed hydrate-based process for juice concentration. The second best and lowest results were obtained for the CO_2 + pineapple system and the CO_2 + grape system.

However, juice systems that presented the small values of CO_2 gas consumption indicate strong inhibiting effects preventing the CO_2 gas from occupying the cages in the hydrate structure. This study claimed that the observed

https://doi.org/10.1021/acsomega.2c01983
ACS Omega 2022, 7, 44591−44602

Table 6. Comparison of the Apparent Rate Constants Derived in This Study with the Literature in Different Juice Systems at T = 275.15 K and Varying Initial Pressures

CO_2 + bitter melon[a]			CO_2 + pineapple[a]			CO_2 + grape[a]		
WC[b] (wt %)	P (MPa)	$K_{app} \times 10^9$	WC[b] (wt %)	P (MPa)	$K_{app} \times 10^9$	WC[b] (wt %)	P (MPa)	$K_{app} \times 10^9$
96.5	3.1131	17.7	91.1	3.5764	17.8	88.5	2.969	12.6
	3.5063	20.1		3.8021	19.0		3.5651	16.3
	4.0739	23.6		4.1672	20.9		3.6282	16.7
97.4	2.8968	17.4	93.3	2.9725	15.2		3.8767	18.3
	3.3897	20.5		3.4297	17.7		3.9391	18.7
	3.908	23.9		3.6157	18.7	91.4	3.0795	14.7
							3.4774	17.4
							3.5146	17.7
							3.5451	18.0

	CO_2 + orange[c]			CO_2 + tomato[d]	
WC[b] (wt %)	P (MPa)	$K_{app} \times 10^9$	WC[b] (wt %)	P (MPa)	$K_{app} \times 10^9$
87.7	1.96	6.70	94.4	1.81	9.40
	2.7	9.70		2.4	13.6
	3.2	13.4		3.1	16.5
	3.72	16.2		3.46	18.2
	4.1	19.1		3.95	20.1

[a]This study [b]Water content. [c]Literature.[21] [d]Literature.[24]

reduction in the number of moles of carbon dioxide gas consumed is due to hydrophilic properties exhibited by juice residuals, meaning that they interact with water molecules via hydrogen bonds. These interactions distort the continuity of water clusters. Therefore, as the number of residuals increases, this increases the number of bonds with water, which reduces the amount of free water that makes hydrate cages leading to reduced gas consumption. As reported in the literature, an increase in water cuts is expected to increase the contact area between water and gas. According to Figures S4 and S6 (Supplementary Material), gas consumption increases with water cuts.

Conversely, there is no observed remarkable increase with the increase in water addition. It can be seen that at higher water cuts of juice, higher initial conditions are required for CO_2 hydrate formation. The increase in residual contents resulted in lower CO_2 consumption, indicating an inhibitory effect of residual contents in investigated juices. As the author varied the juice water cut, it could be concluded that the residual contents, which seem to confirm the hypothesis of juice residuals in inhibiting the hydrate formation, played a crucial role.

5.2.3. Conversion of Water to Hydrates at Different Juice Water Cuts. The effect of varying different initial conditions on the water conversion into hydrates was investigated. Water-to-hydrate conversion as a suitable kinetic parameter was used and is calculated based on the kinetic model proposed by Englezos et al.[38] This kinetic constant is an important parameter affecting the removal efficiency and water recovery. It is important to consider the water because a significant amount of water may remain available at the end of a hydrate formation experiment. This may hinder the commercialization due to increased energy requirements where multiple crystallizers may be required to convert most water to hydrates from the juice. In Tables 3−5, the percentages of water-to-hydrate conversion values for studied systems are reported, and Figures S7−S9 (Supplementary Material) compare these data.

The percentage conversion of water to hydrates was calculated assuming a hydration number of 6.0 for all studied systems. These obtained results demonstrate that the final amount of water converted to hydrates increased as the initial pressure was increased. As shown in Tables 3−5, a similar trend was obtained when decreasing the initial temperature. This indicates that the initial pressure and temperature significantly affect water-to-hydrate conversion. It is expected that an increase and decrease in initial pressure and temperature enable more water to be converted into hydrates. This is due to an increased subcooling temperature. As with the gas consumption results, the highest conversion of water to hydrates was found in the CO_2 + pineapple system, and the lowest was found in the CO_2 + grape system. An increase in juice residuals decreases the water-to-hydrate conversion in all different initial conditions for studied systems.

Meanwhile, the addition of water shows a slight increase in the values of water-to-hydrate conversion. There were several small temperature spikes observed due to hydrate formation. This resulted in increased gas consumption and subsequently led to a higher percentage of water converted to hydrates. The same trend was observed in all other hydrate formation experiments.

5.2.4. Apparent Rate Constant at Different Water Cuts. It was necessary to compare the nucleate growth rates of hydrates under different experimental conditions. The apparent rate constant (K_{app}) as a suitable kinetic parameter for comparison was used and determined based on the kinetic model proposed by Englezos et al.[38] The calculated apparent rate constants under different hydrate conditions were summarized and are listed in Tables 3−5 and shown in Figures S10−S12 (Supplementary Material). As described in the previous section, dissolved solids' combined effects reduce mass transfer and gas consumption rates. As a result, it is expected that mass

https://doi.org/10.1021/acsomega.2c01983
ACS Omega 2022, 7, 44591−44602

and heat transfer rates start to decrease during the hydrate growth stage, which leads to a decrease in the hydrate growth rate. It was observed that at the beginning of the hydrate growth stage, the driving force is maximal, and there are large numbers of stable nuclei due to the presence of dissolved solids of many stable hydrate nuclei. Thus, the apparent rate constant at the beginning of hydrate growth increases and decreases with nuclei' growth. This can be attributed to the exothermic nature of hydrate crystal growth and the reduction of a driving force.

As can be seen, the apparent rate constant increases with the increase in initial conditions (i.e., subcooling). The results indicated that the apparent rate constant increases with the decreasing system temperature. This observed behavior indicates that the system temperature significantly affects this kinetic parameter. Moreover, this demonstrates that better heat transfer benefits the hydrate formation's apparent rate constant under well-mixed conditions. As can be seen, the increase in juice residuals leads to a decrease in the apparent rate constant of CO_2 hydrate growth considerably. This can be attributed to more stable nuclei at the beginning of the hydrate growth stage due to more dissolved solids. Residual solids prohibited hydrate growth, resulting in reduced the apparent rate constant. They are responsible for enhancing the mass transfer by increasing the interfacial tension between the liquid and hydrate phases. The highest apparent rate constant was detected for bitter melon juice under different initial conditions.

5.2.5. Storage Capacity at Different Water Cuts. The storage capacity under different conditions is listed in Tables 3−5 and plotted in Figures S13−S15 (Supplementary Material), allowing easier visualization. As seen in the figures, increasing the initial pressure increases the storage capacity. However, a reverse effect on the storage capacity was observed when the initial temperature was increased from 274.15 to 276.15 K. The behavior shown by these initial conditions signifies that the volume of the stored gas in the hydrate lattice increases with an increase of subcooling, increasing storage capacity.

5.3. Comparison on k_{app}. In an attempt to concentrate juice systems using CO_2 hydrates, Li et al.[21,24] examined the apparent rate constant. In order to validate results obtained with new systems, k_{app} data were compared with literature data derived from kinetic modeling. A comparison of k_{app} data obtained in this study with those measured in the literature[21,24] is presented in Table 6. In addition, Figure S16 illustrates the visual appearance of the same data for the CO_2-based gas hydrate former in different juice systems at T = 275.15 K and varying initial pressures. As seen in Figure S16, a comparison of the trends as expected reveals that higher water cuts lead to the highest apparent rate constant of hydrate growth. It is evident from the observed behavior that one or more compound/s from dissolved solids plays the most critical role in influencing inhibitory effects. Due to agitation, increased thermal conductivity, higher concentrations, and reduced heat and mass transfer resistance may better explain these observed behaviors.[52−54] Moreover, the trends for systems investigated in this study are similar to those reported in the literature.[21,24] The result of high concentrations causes the nuclei to form unstable hydrates at the end of nucleation, and at the beginning of the hydrate growth stage, fewer hydrates can be formed with faster growth rates. In this context, it may be due to fewer nucleation sites, whereas the dissolved solids delay the hydrate formation process.

6. CONCLUSIONS

In this work, the experimental kinetic data of CO_2 hydrate formation in the presence of bitter melon, grape, and pineapple juice were studied to assess the effect of initial conditions on kinetic parameters. The change of initial conditions produced similar effects in all investigated systems. In the light of experimental data obtained in this study, the nature and the composition of constituents and initial conditions (i.e., pressure, temperature, and water cut) emerged as the major factors determining the induction time associated with hydrate formation. Short induction times corresponded to increased subcooling, which initiated CO_2 hydrate formation within the metastable region of CO_2 hydrates. At the higher initial pressures and lower temperatures, the reduction in the onset time of diluted juices systems was much more rapid than that of pure juice.

The overall CO_2 hydrate growth time was increased with increasing juice residuals. It was found that water cuts improved the energy required to form CO_2 gas hydrates. The hydrates formed rapidly under a higher initial condition at all water cuts. As the inhibition effects of investigated systems were weakened, it was observed that CO_2 hydrates formed faster even at higher temperatures. The initial conditions had a significant effect on the kinetic parameters. The amount of CO_2 consumed in the hydrate phase and the growth rate increase with pressure and decrease after reaching a maximum.

From results reported in this study, it can be concluded that a multistage hydrate formation might be used to commercialize the hydrate-based technology for juice concentration. Processing juice with low initial concentration will lead to a more energy efficient and economic concentration process by gas hydrate formation. The nucleation phenomenon of the hydrate phase and its stochastic nature is often cited as a drawback for the industrial application of the hydrate-based process. As each new crystallization step occurs, the liquid phase will need to be recycled so that the memory effect might solve this problem.

■ ASSOCIATED CONTENT

Supporting Information

The Supporting Information is available free of charge at https://pubs.acs.org/doi/10.1021/acsomega.2c01983.

Hydrate formation rate (Figures S1−S3); CO_2 gas consumption (Figures S4−S6); water-to-hydrate conversion (Figures S7−S9); storage capacity (Figures S10−S12); apparent rate constant (Figures S13−S15); and comparison between the apparent rate constant from this study and the literature (Figure S16) (PDF)

■ AUTHOR INFORMATION

Corresponding Author

Kaniki Tumba − *Department of Chemical Engineering, Materials and Separations Research Group (TMSRG), Mangosuthu University of Technology, Durban 4031, South Africa;* orcid.org/0000-0003-2685-3741; Email: tumba@mut.ac.za

Authors

Nkululeko Nkosi − *School of Chemical and Metallurgical Engineering, Oil and Gas Production and Processing Research*

https://doi.org/10.1021/acsomega.2c01983
ACS Omega 2022, 7, 44591−44602

Unit, University of the Witwatersrand, Johannesburg 2001, South Africa; Department of Chemical Engineering, Materials and Separations Research Group (TMSRG), Mangosuthu University of Technology, Durban 4031, South Africa; orcid.org/0000-0002-9151-3359

Diakanua Nkazi − *School of Chemical and Metallurgical Engineering, Oil and Gas Production and Processing Research Unit, University of the Witwatersrand, Johannesburg 2001, South Africa;* orcid.org/0000-0001-8143-705X

Complete contact information is available at: https://pubs.acs.org/10.1021/acsomega.2c01983

Author Contributions

N.N.: conceptualization, formal analysis, investigation, methodology, validation, visualization, and writing original draft. K.T.: supervision, resources, project administration, data curation, and writing review and editing. D.N.: supervision and writing review and editing.

Notes

The authors declare no competing financial interest.

■ ACKNOWLEDGMENTS

This study has been supported by the Mangosuthu University of Technology and the University of Witwatersrand. N.N. wishes to thank the Council for Scientific and Industrial Research (CSIR) in South Africa for the financial support while undertaking this research project.

■ REFERENCES

(1) Hwang, C. C.; Tour, J. J.; Kittrell, C.; Espinal, L.; Alemany, L. B.; Tour, J. M. Capturing Carbon Dioxide as a Polymer from Natural Gas. *Nat. Commun.* **2014**, *5*, 3961.

(2) International Energy Agency. Global Energy Review 2021. *Glob. Energy Rev.* **2020**, *2021*, 1−36.

(3) van Soest, H. L.; den Elzen, M. G. J.; van Vuuren, D. P. Net-Zero Emission Targets for Major Emitting Countries Consistent with the Paris Agreement. *Nat. Commun.* **2021**, *12*, 2140.

(4) Charani Shandiz, S.; Rismanchi, B.; Foliente, G. Energy Master Planning for Net-Zero Emission Communities: State of the Art and Research Challenges. *Renewable Sustainable Energy Rev.* **2021**, *137*, No. 110600.

(5) Lützkendorf, T.; Balouktsi, M. On Net Zero GHG Emission Targets for Climate Protection in Cities: More Questions than Answers? *IOP Conf. Ser. Earth Environ. Sci.* **2019**, *323*, No. 012073.

(6) Mohr, S. H.; Wang, J.; Ellem, G.; Ward, J.; Giurco, D. Projection of World Fossil Fuels by Country. *Fuel* **2015**, *141*, 120−135.

(7) Brockway, P. E.; Owen, A.; Brand-Correa, L. I.; Hardt, L. Estimation of Global Final-Stage Energy-Return-on-Investment for Fossil Fuels with Comparison to Renewable Energy Sources. *Nat. Energy* **2019**, *4*, 612−621.

(8) Mastropietro, P.; Rodilla, P.; Batlle, C. Emergency Measures to Protect Energy Consumers during the Covid-19 Pandemic: A Global Review and Critical Analysis. *Energy Res. Soc. Sci.* **2020**, *68*, No. 101678.

(9) Hughes, A.; Larmour, R. Residential Electricity Consumption in South Africa research report https://www.sanedi.org.za/img/Announcements/June%202021/2021%20Residential%20Electricity%20Consumption%20in%20South%20Africa%20research%20report.pdf.

(10) Ye, Y.; Koch, S. F. Measuring Energy Poverty in South Africa Based on Household Required Energy Consumption. *Energy Econ.* **2021**, *103*, No. 105553.

(11) Ngarava, S.; Zhou, L.; Ningi, T.; Chari, M. M.; Mdiya, L. Gender and Ethnic Disparities in Energy Poverty: The Case of South Africa. *Energy Policy* **2022**, *161*, No. 112755.

(12) Tan, L. S.; Shariff, A. M.; Lau, K. K.; Bustam, M. A. Impact of High Pressure on High Concentration Carbon Dioxide Capture from Natural Gas by Monoethanolamine/N-Methyl-2-Pyrrolidone Solvent in Absorption Packed Column. *Int. J. Greenh. Gas Control* **2015**, *34*, 25−30.

(13) Wilberforce, T.; Olabi, A. G.; Sayed, E. T.; Elsaid, K.; Abdelkareem, M. A. Progress in Carbon Capture Technologies. *Sci. Total Environ.* **2021**, *761*, No. 143203.

(14) Makogon, Y. F. Natural Gas Hydrates − A Promising Source of Energy. *J. Nat. Gas Sci. Eng.* **2010**, *2*, 49−59.

(15) Chong, Z. R.; He, T.; Babu, P.; Zheng, J.; Linga, P. Economic Evaluation of Energy Efficient Hydrate Based Desalination Utilizing Cold Energy from Liquefied Natural Gas (LNG). *Desalination* **2019**, *463*, 69−80.

(16) Ong, C. W.; Chen, C. L. Technical and Economic Evaluation of Seawater Freezing Desalination Using Liquefied Natural Gas. *Energy* **2019**, *181*, 429−439.

(17) Ngema, P. T.; Naidoo, P.; Mohammadi, A. H.; Ramjugernath, D. Phase Stability Conditions for Clathrate Hydrates Formation in CO2 + (NaCl or CaCl2 or MgCl2) + Cyclopentane + Water Systems: Experimental Measurements and Thermodynamic Modeling. *J. Chem. Eng. Data* **2019**, *64*, 4638−4646.

(18) Tumba, K.; Babaee, S.; Naidoo, P.; Mohammadi, A. H.; Ramjugernath, D. Phase Equilibria of Clathrate Hydrates of Ethyne + Propane. *J. Chem. Eng. Data* **2014**, *59*, 2914−2919.

(19) Sergeeva, M. S.; Mokhnachev, N. A.; Shablykin, D. N.; Vorotyntsev, A. V.; Zarubin, D. M.; Atlaskin, A. A.; Trubyanov, M. M.; Vorotyntsev, I. V.; Vorotyntsev, V. M.; Petukhov, A. N. Xenon Recovery from Natural Gas by Hybrid Method Based on Gas Hydrate Crystallisation and Membrane Gas Separation. *J. Nat. Gas Sci. Eng.* **2021**, *86*, No. 103740.

(20) Gambelli, A. M.; Castellani, B.; Nicolini, A.; Rossi, F. Gas Hydrate Formation as a Strategy for CH4/CO2 Separation: Experimental Study on Gaseous Mixtures Produced via Sabatier Reaction. *J. Nat. Gas Sci. Eng.* **2019**, *71*, No. 102985.

(21) Li, S.; Shen, Y.; Liu, D.; Fan, L.; Tan, Z. Concentrating Orange Juice through CO2 Clathrate Hydrate Technology. *Chem. Eng. Res. Des.* **2015**, *93*, 773−778.

(22) Huang, C. P.; Fennema, O.; Powrie, W. D. Gas Hydrates in Aqueous-Organic Systems: II. Concentration by Gas Hydrate Formation. *Cryobiology* **1966**, *2*, 240−245.

(23) Ngan, Y. T.; Englezos, P. Concentration of Mechanical Pulp Mill Effluents and NaCl Solutions through Propane Hydrate Formation. *Ind. Eng. Chem. Res.* **1996**, *35*, 1894−1900.

(24) Li, S.; Shen, Y.; Liu, D.; Fan, L.; Tan, Z.; Zhang, Z.; Li, W.; Li, W. Experimental Study of Concentration of Tomato Juice by CO2 Hydrate Formation. *Chem. Ind. Chem. Eng. Q.* **2015**, *21*, 441−446.

(25) Safari, S.; Varaminian, F. Study the Kinetics and Thermodynamics Conditions for CO2 Hydrate Formation in Orange Juice Concentration. *Innov. Food Sci. Emerg. Technol.* **2019**, *57*, 102155.

(26) Ghiasi, M. M.; Mohammadi, A. H.; Zendehboudi, S. Clathrate Hydrate Based Approach for Concentration of Sugar Aqueous Solution, Orange Juice, and Tomato Juice: Phase Equilibrium Modeling Using a Thermodynamic Framework. *Fluid Phase Equilib.* **2020**, *512*, No. 112460.

(27) Andersen's, T. B.; Thomsen, K.; Andersen, T. B.; Thomsen, K. Separation of Water through Gas Hydrate Formation. *Int. Sugar J.* **2009**, *111*, 632−636.

(28) Doubra, P.; Hassanalizadeh, R.; Naidoo, P.; Ramjugernath, D. Thermodynamic Measurement and Modeling of Hydrate Dissociation for CO2/Refrigerant + Sucrose/Fructose/Glucose Solutions. *AIChE J.* **2021**, 1−11.

(29) Abedi-Farizhendi, S.; Hosseini, M.; Iranshahi, M.; Mohammadi, A.; Manteghian, M.; Mohammadi, A. H. Kinetics of CO 2 Hydrate Formation in Coffee Aqueous Solution: Application in Coffee Concentration. *J. Dispersion Sci. Technol.* **2020**, *41*, 895−901.

(30) Englezos, P. The Freeze Concentration Process and Its Applications. *Dev. Chem. Eng. Miner. Process.* **1994**, *2*, 3−15.

(31) Chun, M. K.; Lee, H. Phase Equilibria of Carbon Dioxide Hydrate System in the Presence of Sucrose, Glucose, and Fructose. *J. Chem. Eng. Data* **1999**, *44*, 1081−1084.
(32) Claßen, T.; Jaeger, M.; Loekman, S.; Gatternig, B.; Rauh, C.; Delgado, A. Concentration of Apple Juice Using CO2 Gas Hydrate Technology to Higher Sugar Contents. *Innov. Food Sci. Emerg. Technol.* **2020**, *65*, No. 102458.
(33) Seidl, P.; Loekman, S.; Sardogan, M.; Voigt, E.; Claßen, T.; Ha, J.; Luzi, G.; Sevenich, R.; Agudo, J. R.; Rauh, C.; Delgado, A. Food Technological Potentials of CO 2 Gas Hydrate Technology for the Concentration of Selected Juices. *High Press. Res.* **2019**, *39*, 344−356.
(34) Smith, A.; Babaee, S.; Mohammadi, A. H.; Naidoo, P.; Ramjugernath, D. Clathrate Hydrate Dissociation Conditions for Refrigerant + Sucrose Aqueous Solution: Experimental Measurement and Thermodynamic Modelling. *Fluid Phase Equilib.* **2016**, *413*, 99−109.
(35) Purwanto, Y. A.; Oshita, S.; Seo, Y.; Kawagoe, Y. Concentration of Liquid Foods by the Use of Gas Hydrate. *J. Food Eng.* **2001**, *47*, 133−138.
(36) Purwanto, Y. A.; Oshita, S.; Seo, Y.; Kawagoe, Y. Separation Process of Nonpolar Gas Hydrate in Food Solution under High Pressure Apparatus. *Int. J. Chem. Eng.* **2014**, *2014*, 1−8.
(37) Li, S.; Qi, F.; Du, K.; Shen, Y.; Liu, D.; Fan, L. An Energy-Efficient Juice Concentration Technology by Ethylene Hydrate Formation. *Sep. Purif. Technol.* **2017**, *173*, 80−85.
(38) Englezos, P.; Kalogerakis, N.; Dholabhai, P. D.; Bishnoi, P. R. Kinetics of Formation of Methane and Ethane Gas Hydrates. *Chem. Eng. Sci.* **1987**, *42*, 2647−2658.
(39) AOAC International. *Official Methods of Analysis of AOAC International - 20th Edition, 2016*, 20th ed.; AOAC: Gaithersbg, 2016.
(40) Sloan, E. D.; Koh, C. A. Clathrate Hydrates of Natural Gases; Chemical Industries; CRC Press; Vol. *20074156*, 2007.
(41) Tumba, K.; Reddy, P.; Naidoo, P.; Ramjugernath, D.; Eslamimanesh, A.; Mohammadi, A. H.; Richon, D. Phase Equilibria of Methane and Carbon Dioxide Clathrate Hydrates in the Presence of Aqueous Solutions of Tributylmethylphosphonium Methylsulfate Ionic Liquid. *J. Chem. Eng. Data* **2011**, *56*, 3620−3629.
(42) Fakir, T.; Babaee, S.; Naidoo, P. Application of Gas Hydrate for the Treatment of Vinasse: Phase Equilibrium and Kinetic Investigations. *J. Chem. Eng. Data* **2021**, *66*, 504−514.
(43) Parrish, W. R.; Prausnitz, J. M. Dissociation Pressures of Gas Hydrates Formed by Gas Mixtures. *Ind. Eng. Chem. Process Des. Dev.* **1972**, *11*, 26−35.
(44) Chen, G.-J.; Guo, T.-M. A New Approach to Gas Hydrate Modelling. *Chem. Eng. J.* **1998**, *71*, 145−151.
(45) Smith, J. M.; Van Ness, H. C.; Abbot, M. M. *Introduction to Chemical Engineering Thermodynamics*, 2000.
(46) Mohammadi, A.; Manteghian, M.; Haghtalab, A.; Mohammadi, A. H.; Rahmati-Abkenar, M. Kinetic Study of Carbon Dioxide Hydrate Formation in Presence of Silver Nanoparticles and SDS. *Chem. Eng. J.* **2014**, *237*, 387−395.
(47) Klauda, J. B.; Sandler, S. I. A Fugacity Model for Gas Hydrate Phase Equilibria. *Ind. Eng. Chem. Res.* **2000**, *39*, 3377−3386.
(48) Dharmawardhana, P. B.; Parrish, W. R.; Sloan, E. D. Experimental Thermodynamic Parameters for the Prediction of Natural Gas Hydrate Dissociation Conditions. *Ind. Eng. Chem. Fundam.* **1980**, *19*, 410−414.
(49) Zhang, J. S.; Lee, S.; Lee, J. W. Kinetics of Methane Hydrate Formation from SDS Solution. *Ind. Eng. Chem. Res.* **2007**, *46*, 6353−6359.
(50) Kashchiev, D.; Firoozabadi, A. Induction Time in Crystallization of Gas Hydrates. *J. Cryst. Growth* **2003**, *250*, 499−515.
(51) Bowick, M. J.; Travesset, A. The Statistical Mechanics of Membranes. *Phys. Rep.* **2000**, *344*, 255−308.
(52) Tajima, H.; Yamasaki, A.; Kiyono, F. Effects of Mixing Functions of Static Mixers on the Formation of CO2 Hydrate from the Two-Phase Flow of Liquid CO2 and Water. *Energy Fuels* **2005**, *19*, 2364−2370.
(53) Uchida, T.; Ikeda, I. Y.; Takeya, S.; Ebinuma, T.; Nagao, J.; Narita, H. CO2 Hydrate Film Formation at the Boundary between CO2 and Water: Effects of Temperature, Pressure and Additives on the Formation Rate. *J. Cryst. Growth* **2002**, *237*−*239*, 383−387.
(54) Yang, D.; Le, L. A.; Martinez, R. J.; Currier, R. P.; Spencer, D. F. Kinetics of CO2 Hydrate Formation in a Continuous Flow Reactor. *Chem. Eng. J.* **2011**, *172*, 144−157.

https://doi.org/10.1021/acsomega.2c01983
ACS Omega 2022, 7, 44591−44602